Journal of Marine Science and Technology

Volume 30 | Issue 6 Article 5

Optimization of Circular Silencers Internally Hybridized with Multiple Reverse Chambers Using the GA Method

Min-Chie Chiu
Department of Mechanical and Materials Engineering, Tatung University, Taipei, 10452, Taiwan, ROC,
minchie.chiu@msa.hinet.net

Ying-Chun Chang
Department of Mechanical and Materials Engineering, Tatung University, Taipei, 10452, Taiwan, ROC

Tian-Syung Lan
Department of Information Management, Yu Da University of Science and Technology, Miaoli County, 361, Taiwan, ROC

Ho-Sheng Chen
College of Mechatronic Engineering, Guangdong University of Petrochemical Technology, Maoming 525000, Guangdong, China

Recommended Citation

Chiu, Min-Chie; Chang, Ying-Chun; Lan, Tian-Syung; and Chen, Ho-Sheng (2022) "Optimization of Circular Silencers Internally Hybridized with Multiple Reverse Chambers Using the GA Method," *Journal of Marine Science and Technology*: Vol. 30: Iss. 6, Article 5.
DOI: 10.51400/2709-6998.2587
Available at: https://jmstt.ntou.edu.tw/journal/vol30/iss6/5

RESEARCH ARTICLE

Optimization of Circular Silencers Internally Hybridized with Multiple Reverse Chambers Using the GA Method

Min-Chie Chiu [a,*], Ying-Chun Chang [a], Tian-Syung Lan [b], Ho-Sheng Chen [c]

[a] Department of Mechanical and Materials Engineering, Tatung University, Taipei, 10452, Taiwan, ROC
[b] Department of Information Management, Yu Da University of Science and Technology, Miaoli County, 361, Taiwan, ROC
[c] College of Mechatronic Engineering, Guangdong University of Petrochemical Technology, Maoming 525000, Guangdong, China

Abstract

A noise abatement method using an eigen function in conjunction with an optimizer (Genetic Algorithm) under a space-constrain situation is proposed in this study concerning a high order wave propagation effect. An eigen function is used to describe an acoustical field and shorten the acoustical model in a four-pole transfer matrix form. The system's four-pole matrix estimates the Transmission Loss (TL) for the silencers by multiplying individual four-pole matrices.

Additionally, a case study of an air compressor's broadband noise elimination is introduced. Three types of circular reverse silencers (silencers A-C) internally hybridized with multiple straight chambers are adopted to efficiently suppress the noise wave. Considering broadband characteristics and space-constrained situations, an average-deviation-integrating form used as an objective function is presented and linked to an optimizer-GA (Genetic Algorithm). Acoustical models for silencers A to C are checked before the numerical optimization is performed. A pure tone optimization is executed to assure the consistency of the GA scheme. The result shows that the overall noise drop is enhanced and the number of straight expansion chambers installed at the inlet/outlet of the circular reverse silencer increases. Consequently, concerning a space-constrained situation in the real world and the characteristics of the broadband noise spectrum, an efficient method is proposed in this paper for designing an optimally shaped hybrid muffler using the objective function in conjunction with an optimization scheme.

Keywords: Eccentrics, Genetic algorithm, High order wave, Optimization, Reverse

1. Introduction

A number of studies on mufflers used in venting noise have been thoroughly examined. Munjal [1] established a four-pole transfer matrix to estimate the noise reduction based on fluid dynamics theory. Sullivan and Crocker [2,3] developed coupled equations for a perforated muffler at outer and inner tubes. However, the acoustical effect of a high order wave was neglected in the studies mentioned above. Therefore, Ih and Lee [4] developed a mathematical model of an expansion chamber with a circular section and mean flow. Yi and Lee [5,6] presented a theoretical scheme to forecast the acoustical efficiency of expansion chamber mufflers in circular shape and hybridized with straight/side inlets and outlets.

Ih and Lee [7] offered a scheme for predicting the noise reduction of the circular-sectioned reverse silencers. A numerical assessment was performed to shorten the estimation of an expansion silencer organized with two segments (rectangular and circular) [8]; however, the analysis using the scheme at the condition of 90° angle between the inlet and the outlet proved difficult. Selamet and Ji [9] investigated the acoustic reduction of circular-sectioned flow-reversing chambers. A one-expansion-chamber silencer with an elliptical section was proposed by Mimani and Munjal [10] based on plane wave model and analyzed. Ranjbar et al. [11] assessed the

Received 8 April 2022; revised 24 May 2022; accepted 11 August 2022.
Available online 10 December 2022

* Corresponding author. Department of Mechanical and Materials Engineering, Tatung University, No.40, Sec.3, Zhongshan N. Rd., Taipei, 10452, Taiwan, R.O.C.
E-mail address: mcchiu@gm.ttu.edu.tw (M.-C. Chiu).

https://doi.org/10.51400/2709-6998.2587

best design within a limited time for structural acoustics. Subsequently, an automotive silencer's acoustical fluid-dynamic optimization was assessed by Siano et al. [12] based on the plane wave model. Mimani and Munjal [13] proposed a semi-analytical method that utilized Green's function in conjunction with driven uniform-piston model to predict the end-correction length effect within an axial and long reversal chamber. Arslan et al. [14] investigated muffler design for transmitted noise reduction in 2018. Mohamad et al. [15] investigated Formula racecar exhaust mufflers using a hybrid technique. Arslan et al. [16] analyzed a multi-chamber reactive silencer in 2020. Later, Arslan et al. [17] explored maximum sound transmission loss in multi-chamber reactive silencers. Mohamad et al. explored the acoustical effect of perforated tubes for three-dimensional exhaust mufflers with mean flow [18].

In dealing with venting systems' industrial noise, a multi-chamber muffler has been utilized to suppress sound energy. However, the multi-chamber muffler design and optimization assessment of mufflers in constrained conditions still has not been considered. In 2010, Chiu [19–22] proposed an optimal assessment on multi-chamber mufflers hybridized with perforated intruding inlets and resonated tubes. The optimization of reverse-flow mufflers and multi-chamber mufflers with the plug-inlet tubes in a venting process. Numerical optimization of acoustical performance for hybrid mufflers under back pressure constrained. Also, the shape optimization of three-chamber hybrid mufflers within constrained backpressure and space in 2012. Chiu [23,24] provided a numerical assessment method for dealing with broadband noise and pure tone using a hybrid muffler and simulated the annealing method in 2013. Ranjbar and Kemani [25] presented an optimization of muffler design by genetic algorithm and random search method. Mohamad et al. [26] presented the hybrid method technique and transfer matrix method in vehicle muffler optimization in 2021.

The above mentioned studies are focused mainly on analyzing acoustical waves at low and medium frequencies. Some research the use of both boundary element method (BEM) and finite element method (FEM) has also been addressed in some studies of high order wave modes [27–32]. Chiu and Chang [33] have discussed the optimization of a simple expansion chamber silencer in a high-order mode in 2014. Nevertheless, extensive calculation time for muffler modeling is required. Difficulty in running the FEM software for optimum is also a problem. Therefore, to increase the muffler's acoustical efficiency under a space-limited condition, an optimization of circular mufflers hybridized with multiple reverse cavities using the eigen function together with the genetic algorithm method was considered [34]. Three circular hybrid silencers (A, a one-chamber silencer hybridized with one reverse chamber; B, a three-chamber silencer hybridized with two straight chambers and one reverse chamber; and C, a five-chamber silencer hybridized with four straight chambers and one reverse chamber) are presented and optimized with the GA optimizer.

Nomenclature

The following symbols are used herein for the purpose of this paper:

a, R_3	expansion chamber's radius
aa_1, R_2	reverse chamber inlet's radius
aaa_1, R_5	reverse chamber outlet's radius
a_1, R_1	inlet's radius
a_2, R_4	outlet's radius
c_0	sound speed (m/s)
d	expansion chamber's diameter
e_1, E_1	the distance between the inlet and the expansion chamber
e_2, E_2	the distance between the outlet and the expansion chamber
f	requency (Hz)
$\text{iter}_{\max}$	extreme iteration in GA's optimization
J_n	n-order Jacobsthal polynomial series
k	sound's wave number $\left(\frac{\omega}{c_o}\right)$
k_r	sound's wave number in r-axis $\left(\frac{\omega_r}{c_o}\right)$
k_z	sound's wave number in z-axis $\left(\sqrt{k^2/k_r^2}\right)$
L_1, L_2, L_3, L	expansion chamber's length
m, n	acoustical mode
$\overline{p}_{ii}$	an average acoustical pressure (Pa)
$\overline{p}_{li}$	an average internally communicating acoustical pressure (Pa)
$\overline{P}_1$	inlet's acoustical potential energy
$\overline{P}_2$	outlet's acoustical potential energy
pc	crossover rate
pm	mutation rate
pp	population number
$SWLO_i$	unsilenced sound power level at ith (1/1) octave band frequency
SWL_i	silenced sound power level at ith (1/1) octave band frequency
TL_i	silencer's TL with respect to the relative octave band frequency
U_i	volume velocity (m/s)
Z_0	expansion chamber's acoustical impedance at inlet
θ, θ_0	angles between inlet and outlet
ω	angular frequency ($=2\pi f$) (rad/s)
ρ_0	density of air (kg/m^3)

2. Mathematical background

To establish the theoretical models for silencers A, B and C, an eigen function which uses both 3-D wave propagation and orthogonal eigen mode is adopted to

simplify the acoustical model into a four-pole transfer matrix. Individual matrices used to evaluate the silencer's Transmission Loss (TL), are multiplied to form an overall system's four-pole matrix. The mathematical models of acoustical elements (reverse chamber and straight chamber) in various configurations and silencers Ã C are described below.

2.1. Acoustical model for a circular-sectioned silencer hybridized with one reverse chamber

First, the acoustical model for a circular-sectioned muffler hybridized with one reverse-chamber according to wave propagation in higher order mode is depicted in Fig. 1. The sound pressure at both inlet and outlet is averaged according to the eigen function deduced from Ih & Lee [4] and Yi & Lee [5,6].

$$\overline{p}_{ii} = (-1)^{i-1} jU_i Z\left\{\cot kL + \left(\frac{2a}{\lambda_{nm} a_i}\right)^2 \sum_n{}' \sum_m{}' \frac{k\cot k_{z_{nm}} L J_n^2(\lambda_{nm} e_i/a) J_1^2(\lambda_{nm} a_i/a)}{k_{z_{nm}}(1-n^2/\lambda_{nm}^2) J_n^2(\lambda_{nm})\lambda_{nm}^2}\right\} \tag{1}$$

$$\overline{p}_{li} = (-1)^{i} jU_i Z\left\{\cot kL + 4\left(\frac{a}{a_i}\right)\left(\frac{a}{a_l}\right) \sum_n{}' \sum_m{}' \frac{k\cot k_{z_{nm}} L J_1(\lambda_{nm} a_i/a) J_1(\lambda_{nm} a_l/a)}{k_{z_{nm}}(1-n^2/\lambda_{nm}^2) J_n^2(\lambda_{nm})\lambda_{nm}^2}\right\}$$
$$= (-1)^{l} jU_i Z E_{li}$$

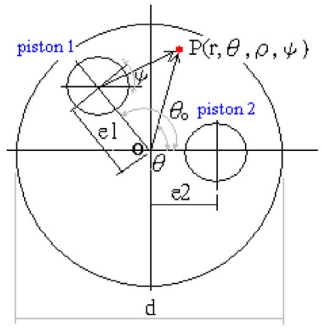

(a) Cross section of the circular silencer with one reverse chamber.

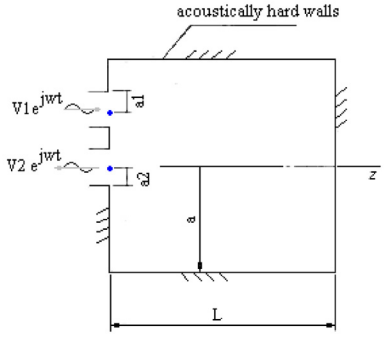

(b) Side view of the circular silencer with one reverse chamber.

Fig. 1. Mechanism of the circular silencer with one reverse chamber (Ih and Lee, 1987; Yi and Lee, 1987).

$$(i = 1 \text{ and } l = 2) \text{ or } (i = 2 \text{ and } l = 1) \tag{2}$$

For inlet part, the total acoustical potential energy yields

$$\overline{P}_1 = \overline{p}_{11} + \overline{p}_{12} = -jZ_0(U_1 E_{11} - U_2 E_{12}) \tag{3}$$

For outlet part, the total acoustical potential energy yields

$$\overline{P}_2 = \overline{p}_{21} + \overline{p}_{22} = -jZ_0(U_1 E_{21} - U_2 E_{22}) \tag{4}$$

Joining Eq. (3) with Eq. (4) yields

$$\begin{bmatrix} P_1 \\ U_1 \end{bmatrix} = \begin{bmatrix} T_{11} & T_{12} \\ T_{21} & T_{22} \end{bmatrix} \begin{bmatrix} P_2 \\ U_2 \end{bmatrix} \tag{5}$$

By expanding Eq. (5), the following is obtained:

$$\begin{aligned} P_1 &= T_{11} P_2 + T_{12} U_2 \\ U_1 &= T_{21} P_{2+} T_{22} U_2 \end{aligned} \tag{6}$$

The related pole is obtained as

$$\begin{aligned} T_{11} &= (\overline{P}_1/\overline{P}_2)|_{U_2=0} = E_{11}/E_{12}, \\ T_{12} &= (\overline{P}_1/U_2)|_{\overline{P}_2=0} = jZ_0(E_{12} - E_{11}E_{22}/E_{12}) \\ T_{21} &= (U_1/\overline{P}_2)|_{U_2=0} = j(Z_0 E_{12})^{-1}, \\ T_{22} &= (U_1/U_2)|_{\overline{P}_2=0} = E_{22}/E_{12} \end{aligned} \tag{7}$$

The sound TL of a circular-sectioned silencer hybridized with a reverse chamber at nodes 1 and 2 is [35].

$$TL = 20\log\left(\frac{|T_{11} + T_{12} + T_{21} + T_{22}|}{2}\right) + 10\log\left(\frac{S_{in}}{S_{out}}\right) \tag{8a}$$

where

$$Z_0 = \rho_0 c/\pi a_1^2 \tag{8b}$$

2.2. Acoustical model for a circular-sectioned and one-chamber straight silencer at the same axes of inlet and outlet

The acoustical model of a circular-sectioned straight-silencer having one chamber based on wave

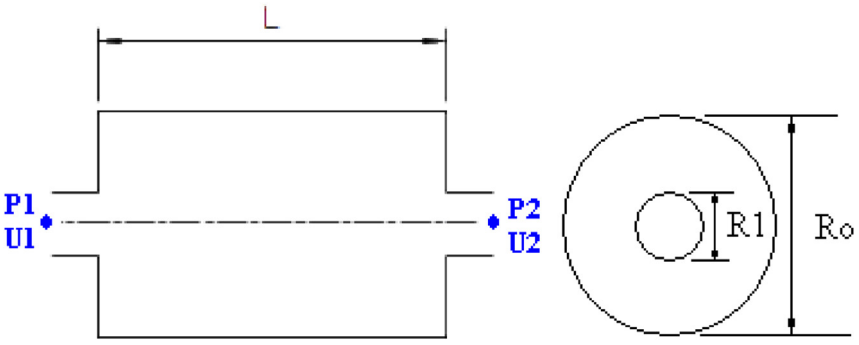

Fig. 2. Mechanism of the circular and one-chamber straight silencer (Ih and Lee, 1985; Yi and Lee, 1986).

propagation theory in higher-order mode is provided in Fig. 2. Given to eigen function from Munjal [8], Ih & Lee [4], and Yi & Lee [5,6], averaged sound pressures at both silencer's inlet and outlet are

$$\overline{p}_{ii} = (-1)^{i-1} U_i Z \left\{ \frac{1}{\tan kL} - \left(\frac{a}{a_i}\right)^2 \sum_n{}' \sum_m{}' \frac{4kJ_1^2(\lambda_{nm}a_i/a) J_n^2(\lambda_{nm}\delta_i/a)}{(-1)k_{z_{nm}}(1-n^2/\lambda_{nm}^2)\tan(k_{z_{nm}}L) J_n^2(\lambda_{nm})\lambda_{nm}^2} \right\} = (-1)^{i-1} U_i Z E_{ii} \quad (9)$$

$(i = 1 \text{ or } 2)$

$$\overline{p}_{il} = (-1)^{i-1} U_i Z \left\{ \frac{1}{\sin kL} - \left(\frac{a}{a_1}\right)\left(\frac{a}{a_2}\right) \sum_m{}' \sum_n{}' \left[4k \cos n\theta_o J_1\left(\frac{\lambda_{nm}a_1}{a}\right) J_1\left(\frac{\lambda_{nm}a_2}{a}\right) J_n\left(\frac{\lambda_{nm}\delta_1}{a}\right) J_1\left(\frac{\lambda_{nm}\delta_2}{a}\right) \right] \right.$$
$$\left. \times \left[(-1)k_{z_{nm}} \left(1 - \frac{n^2}{\lambda_{nm}^2}\right) \sin(k_{z_{nm}}L) J_n^2(\lambda_{nm}) \lambda_{nm}^2 \right]^{-1} \right\} = (-1)^i U_l Z E_{il} \quad (10)$$

$(i = 1 \text{ and } l = 2) \text{or} (i = 2 \text{ and } l = 1)$

In case that both silencer's inlet and outlet are at the same axis, the sound pressure yields

$$\overline{p}_{ii} = (-1)^{i-1} U_i Z \left\{ \frac{1}{\tan kl} - \left(\frac{a}{a_i}\right)^2 \sum_{m=1}^{\infty} \frac{4kJ_1{}^2(\lambda_{0m}a_i/a)}{(-1)k_{z_{0m}} \tan(k_{z_{0m}}l) J_0{}^2(\lambda_{0m}) \lambda_{0m}{}^2} \right\} \quad (11)$$
$$\equiv (-1)^{i-1} U_i Z E_{ii} \quad (i = 1 \text{ or } 2)$$

$$\overline{p}_{il} = (-1)^{i-1} U_i Z \left\{ \frac{1}{\sin kL} - \left(\frac{a}{a_1}\right)\left(\frac{a}{a_2}\right) \sum_{m=1}^{\infty} \left[4kJ_1\left(\frac{\lambda_{0m}a_1}{a}\right) J_1\left(\frac{\lambda_{0m}a_2}{a}\right) \right] \times \left[(-1)k_{z_{0m}} \sin(k_{z_{0m}}L) J_0^2(\lambda_{0m}) \lambda_{0m}^2 \right]^{-1} \right\} = 1 \quad (12)$$
$$= (-1)^i U_l Z E_{il}$$
$$(i = 1 \text{ and } l = 2) \text{ or } (i = 2 \text{ and } l = 1)$$

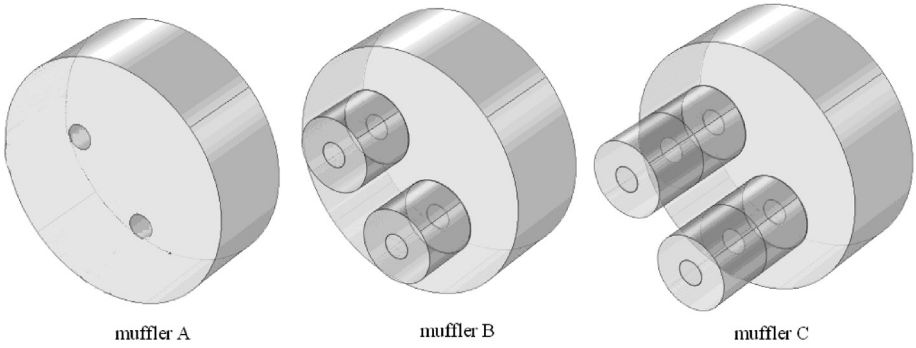

Fig. 3. The mechanism for three silencers (silencer A: one reverse chamber; silencer B: three reverse chambers; silencer C: five reverse chambers).

2.3. Transmission loss of mufflers A-C

Figure 3 shows three categories of circular mix silencers (silencer A: a silencer hybridized with one reverse chamber, silencer B: a silencer hybridized with three reverse chambers, and silencer C: a silencer hybridized with five reverse chambers).

The acoustical performance of silencers A-C is established based on the acoustical model mentioned above and presented as follows:

The acoustical fields of silencer A to silencer C are shown in Fig. 4. For silencer A, two points are chosen to demonstrate the sound field of the entire silencer.

The organism's matrix and its TL are described below:

$$\begin{bmatrix} P_1 \\ U_1 \end{bmatrix} = \prod_{m=1}^{1} [T_m(f)] \begin{bmatrix} P_2 \\ U_2 \end{bmatrix}$$

$$\begin{bmatrix} T_{T11} & T_{T12} \\ T_{T21} & T_{T22} \end{bmatrix} \begin{bmatrix} P_2 \\ U_2 \end{bmatrix} \tag{13a}$$

$$TL_1(f, \overline{X}_1) = 20\log\left[\frac{|T_{T11} + T_{T12} + T_{T21} + T_{T22}|}{2}\right] + 10\log\left(\frac{S_1}{S_2}\right) \tag{13b}$$

$$\overline{X}_1 = (KT_1, KT_2, KT_3, KT_4, KT_5, KT_6) \tag{13c}$$

where

$KT_1 = a_1$; $KT_2 = a_2$; $KT_3 = e_1$; $KT_4 = e_2$; $KT_5 = L_2$; $KT_6 = \theta$ **(13d)**

Similarly, for silencer B, four points are chosen to exemplify the sound field of the complete muffler. The organism's matrix and its TL yield

$$\begin{bmatrix} P_1 \\ U_1 \end{bmatrix} = \begin{bmatrix} TS1_{1,1} & TS1_{1,2} \\ TS1_{2,1} & TS1_{2,2} \end{bmatrix} \begin{bmatrix} TR1_{1,1} & TR1_{1,2} \\ TR1_{2,1} & TR1_{2,2} \end{bmatrix} \begin{bmatrix} TS2_{1,1} & TS2_{1,2} \\ TS2_{2,1} & TS2_{2,2} \end{bmatrix} \begin{bmatrix} P_4 \\ U_4 \end{bmatrix}$$

$$= \begin{bmatrix} T_{T11} & T_{T12} \\ T_{T21} & T_{T22} \end{bmatrix} \begin{bmatrix} p_4 \\ U_4 \end{bmatrix} \tag{14a}$$

$$TL_2(f, \overline{X}_2) = 20\log\left[\frac{|T_{T11} + T_{T12} + T_{T21} + T_{T22}|}{2}\right] + 10\log\left(\frac{S_1}{S_4}\right) \tag{14b}$$

$$\overline{X}_2 = (KT_1^*, KT_2^*, KT_3^*, KT_4^*, KT_5^*, KT_6^*, KT_7^*, KT_8^*) \tag{14c}$$

where

$KT_1^* = a_1/aa_1$; $KT_2^* = a_2/aaa_1$; $KT_3^* = e_1$; $KT_4^* = e_2$; $KT_5^* = L_2/L_o$; $KT_6^* = \theta$; $KT_7^* = aa_1$; $KT_8^* = aaa_1$; $L_1 = L_o - L_2$ **(14d)**

Likewise, for silencer C, the system's matrix and its TL presented by six nodes are

$$\begin{bmatrix} P_1 \\ U_1 \end{bmatrix} = \prod_{m=1}^{5} [T_m(f)] \begin{bmatrix} P_6 \\ U_6 \end{bmatrix}$$

$$= \begin{bmatrix} T_{T11} & T_{T12} \\ T_{T21} & T_{T22} \end{bmatrix} \begin{bmatrix} P_6 \\ U_6 \end{bmatrix} \tag{15a}$$

$$TL_3(f, \overline{X}_3) = 20\log\left[\frac{|T_{T11} + T_{T12} + T_{T21} + T_{T22}|}{2}\right] + 10\log\left(\frac{S_1}{S_6}\right) \tag{15b}$$

$$\overline{X}_3 = (KT_1^{**}, KT_2^{**}, KT_3^{**}, KT_4^{**}, KT_5^{**}, KT_6^{**}, KT_7^{**}, KT_8^{**}, KT_9^{**}) \tag{15c}$$

where m is the number of chambers,

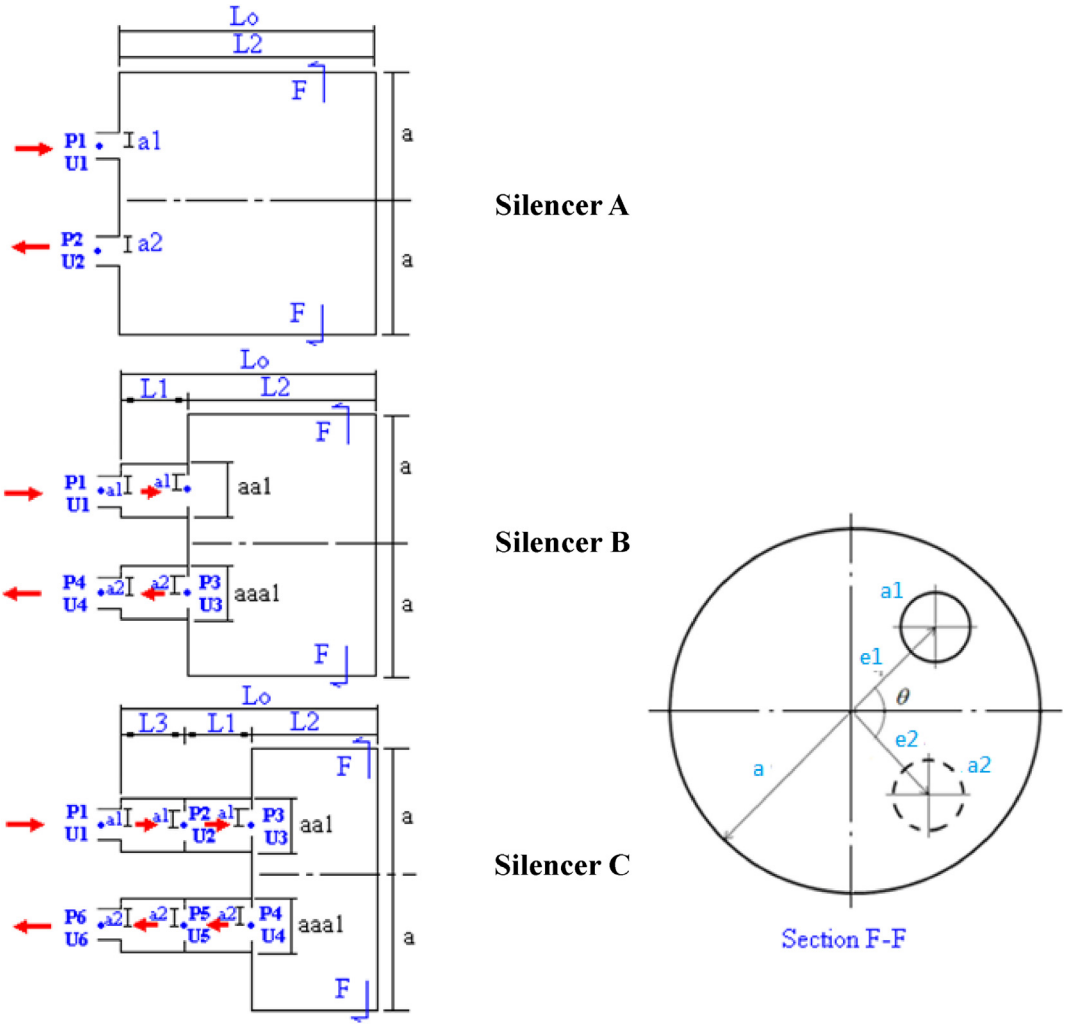

Fig. 4. The acoustical fields of three silencers (silencer A: one reverse chamber; silencer B: three reverse chambers; silencer C: five reverse chambers).

KT_1** = a_1/aa_1; KT_2** = a_2/aaa_1; KT_3** = e_1; KT_4** = e_2; KT_5** = L_2/L_o; KT_6** = θ; KT_7** = aa_1; KT_8** = aaa_1; KT_9** = $L_1/(L_o - L_2)$; L_1=(1- KT_5)*L_o* KT_9**; $L_3 = L_o - L_1 - L_2$ (15d)

2.4. Objective function

Three OBJ functions are developed to suppress the broadband SWL (Sound Power Level) emitted by venting noise, as illustrated below:

The silenced octave sound power level emitted from silencer's outlet is

$$SWL_i = SWLO_i - TL_i \tag{16}$$

where

(1) $SWLO_i$ is the original SWL at inlet of silencer (or pipe outlet), and i is the index of octave band frequency.
(2) TL_i is the silencer's TL with respect to the relative octave band frequency.
(3) SWL_i is the silenced SWL at outlet of silencer with respect to the relative octave band frequency.

Finally, the overall SWL_T silenced by silencers A~C at outlet is selected as the objective function

Silencer A:

$$OBJ_1(\overline{X}_1) = SWL_{1(T)}$$

$$= 10\log\left\{\sum_{i=1}^{7} 10^{-TL_1(f=31.5)]/10^{+}} {}^{[SWLO(f=31.5)} 10^{-TL_1(f=63)]/10^{+}} {}^{[SWLO(f=63)} 10^{-TL_1(f=125)]/10^{+}} {}^{[SWLO(f=125)} 10^{-TL_1(f=250)]/10^{+}} {}^{[SWLO(f=250)} 10^{-TL_1(f=500)]/10^{+}} {}^{[SWLO(f=500)} 10^{-TL_1(f=1000)]/10^{+}} {}^{[SWLO(f=1000)} 10^{-TL_1(f=2000)]/10} {}^{[SWLO(f=2000)}\right\} \tag{17a}$$

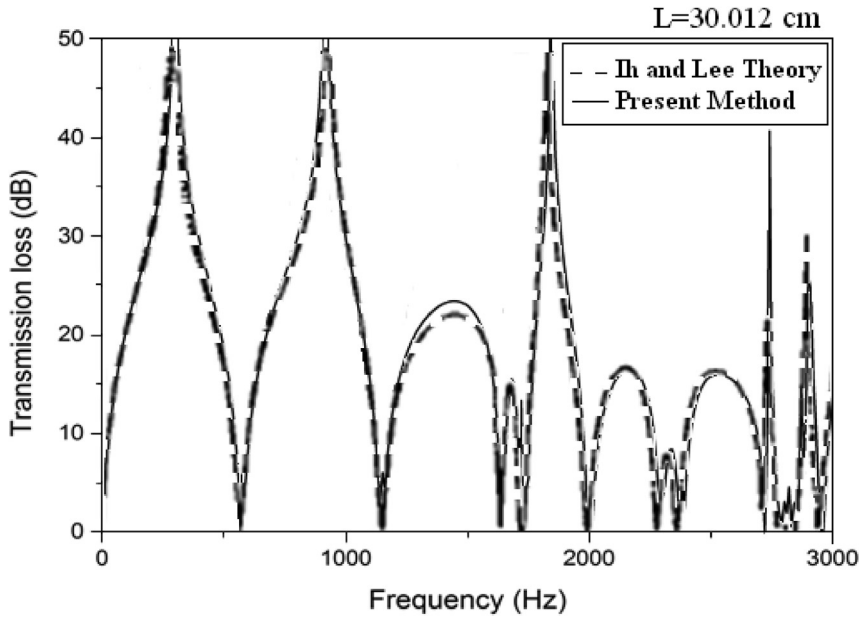

Fig. 5. Accuracy check of silencer A's mathematical model by using analytic data from Ih and Lee (1987).

Silencer B:

$$OBJ_2(\overline{X}_2) = SWL_{2(T)}$$

$$= 10\log\left\{\sum_{i=1}^{7} 10^{\begin{matrix}[SWLO(f=31.5) & [SWLO(f=63) & [SWLO(f=125) & [SWLO(f=250) \\ -TL_2(f=31.5)]/10 & +\ -TL_2(f=63)]/10 & +\ 10^{-TL_2(f=125)]/10} & +\ 10^{-TL_2(f=250)]/10}\end{matrix}} \right.$$

$$\left. \begin{matrix}[SWLO(f=500) & [SWLO(f=1000) & [SWLO(f=2000) \\ 10^{-TL_2(f=500)]/10} & +\ 10^{-TL_2(f=1000)]/10} & +\ 10^{-TL_2(f=2000)]/10}\end{matrix} \right\} \tag{17b}$$

Silencer C:

$$OBJ_3(\overline{X}_3) = SWL_{3(T)}$$

$$= 10\log\left\{\sum_{i=1}^{7} 10^{\begin{matrix}[SWLO(f=31.5) & [SWLO(f=63) & [SWLO(f=125) & [SWLO(f=250) \\ -TL_3(f=31.5)]/10 & +\ -TL_3(f=63)]/10 & +\ 10^{-TL_3(f=125)]/10} & +\ 10^{-TL_3(f=250)]/10}\end{matrix}} \right.$$

$$\left. \begin{matrix}[SWLO(f=500) & [SWLO(f=1000) & [SWLO(f=2000) \\ 10^{-TL_3(f=500)]/10} & +\ 10^{-TL_3(f=1000)]/10} & +\ 10^{-TL_3(f=2000)]/10}\end{matrix} \right\} \tag{17c}$$

3. Acoustical model verification

Before executing the *GA*'s numerical assessment on the circular-sectioned silencers hybridized with multiple reverse chambers, the acoustical mathematical simulation for silencer A (a circular−sectioned silencer hybridized with one reverse chamber) is verified by the analytical data from Ih and Lee [7]. In Fig. 5, the result shows consistency between both of them. The acoustical models of silencers B and C is checked for accuracy using FEM analysis (run by COMSOL), as shown in Figs. 6 and 7. The figures reveal that the method proposed is roughly in line with the FEM's data. Consequently, the acoustical

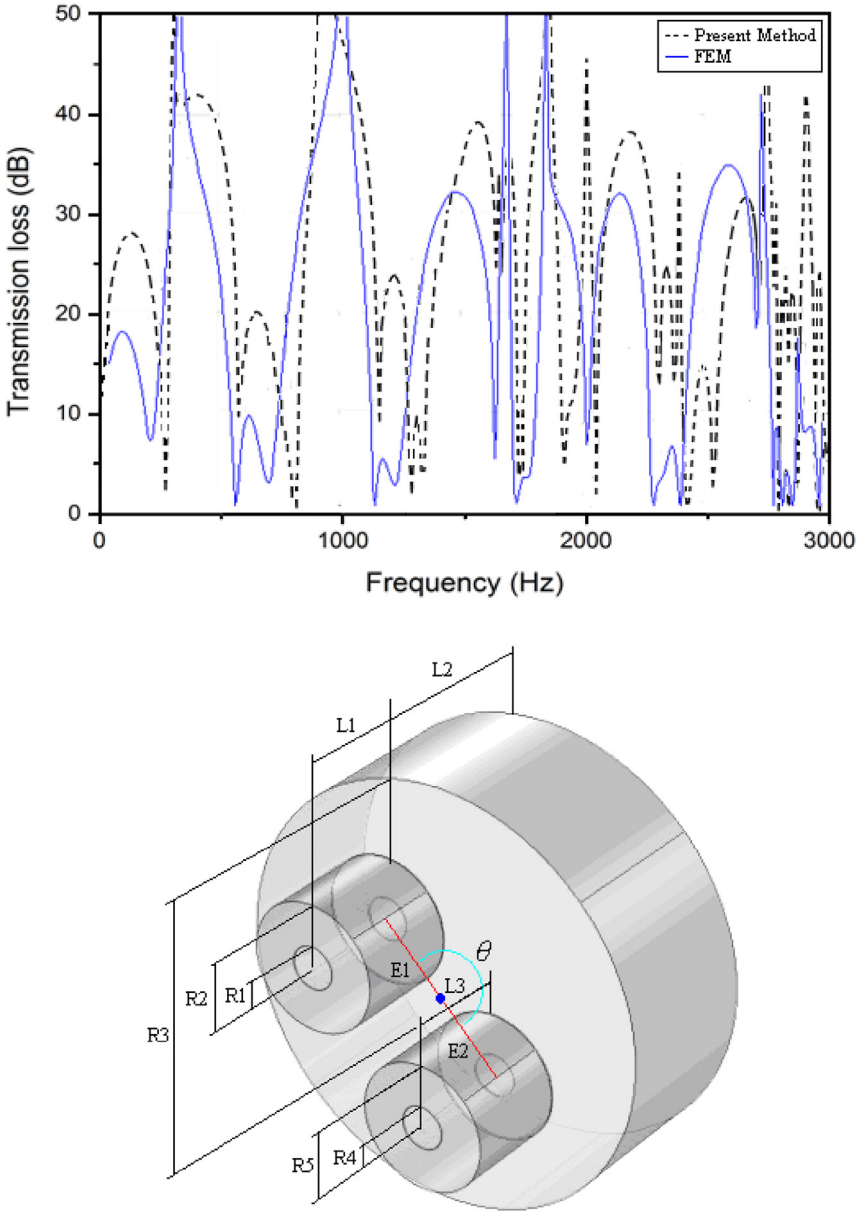

Fig. 6. Accuracy check of silencer B's mathematical model using the FEM analysis run by COMSOL (L1 = L2 = L3 = 30.012 cm; R1 = 1.0209 cm, R2 = 2.091 cm, R3 = 6.15 cm, R4 = 1.0209 cm, R5 = 2.091 cm, E1 = E2 = 4.182 cm, θ = 180°).

models of silencer A to silencer C allied by the numerical method are adopted in the optimization process in the following section.

4. Case study

A silencer confined within an air compressor package is depicted in Fig. 8(a). The SWL (Sound Power Level) spectrum discharged from the outlet of the air compressor is illustrated in Fig. 8 (b). To efficiently suppress the broadband noise, three circular-sectioned and multi-chamber silencers depicted in Fig. 3 and Eq. (17) (a)–(c) are used in conjunction with the GA method. Figure 1 shows that the permitted zone for a silencer is 0.123 m in diameter and 0.35 m in length. The dimension constraints and range of parameters for each silencer are listed in Table 1. To validate the GA's reliability in silencer optimization, a *TL*'s maximization regarding silencers A-C at a specified tone of 300 Hz is carried out before minimizing broadband noise. The objective functions with concerning silencer A to silencer C are listed below:

Silencer A:

$$OBJ_{01}\left(f,\overline{X}_1\right)=TL_1(\overline{X}_1)_{f=300Hz} \tag{18a}$$

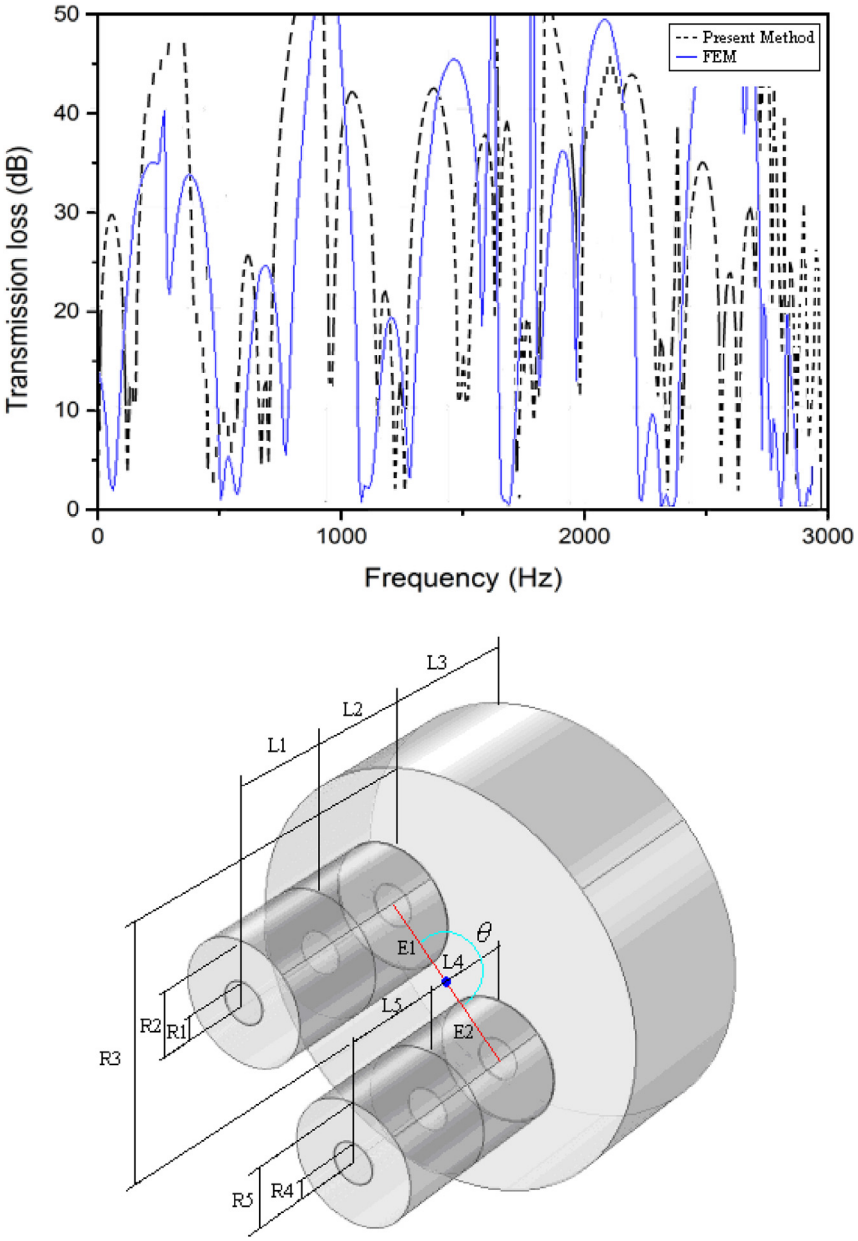

Fig. 7. Accuracy check of silencer C's mathematical model using the FEM analysis run by COMSOL (L1 = L2 = L3 = L4 = L5 = 30.012 cm, R1 = 1.0209 cm, R2 = 2.091 cm, R3 = 6.15 cm, R4 = 1.0209 cm, R5 = 2.091 cm, E1 = E2 = 4.182 cm, θ = 180°).

Silencer B:

$$OBJ_{02}(f,\overline{X}_2) = TL_2(\overline{X}_2)_{f=300Hz} \tag{18b}$$

Silencer C:

$$OBJ_{03}(f,\overline{X}_3) = TL_3(\overline{X}_3)_{f=300Hz} \tag{18c}$$

5. Genetic algorithm

The genetic algorithm (GA) is a robust search algorithm created by Holland [36] and improved by Jong [37] as an optimization function. It finds the global optimum value through the process of genetic evolution. Figure 9 shows the working principle of genetic algorithm. As shown in Fig. 9, several strategies are used in the gene's elite program, including tournament selection and fitness comparison of randomly selected pairs of chromosomes. In addition, a uniform crossover with a probability *pc* and a mutation scheme for expanding the gene pool species with probability *pm* are employed. As shown in Fig. 10, the *GA* process is completed when the number $iter_{\max}$ reaches an extreme value.

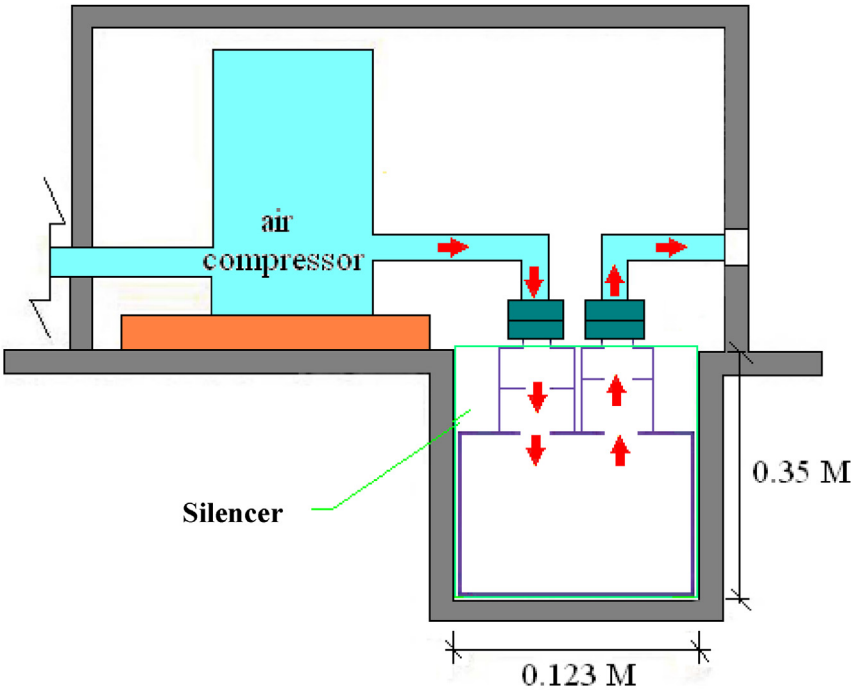

(a) A space-constrained air compressor package.

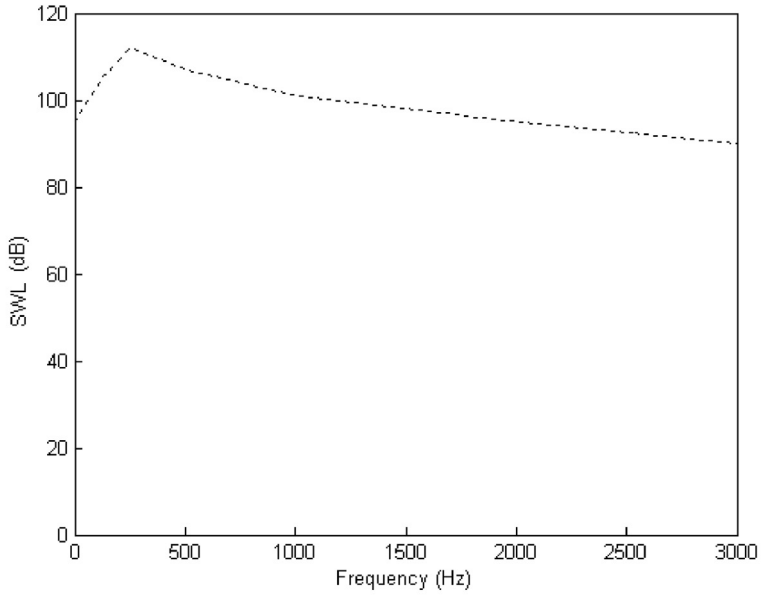

(b) SWL spectrum of the air compressor (overall SWLO=127.1 dB).

Fig. 8. An air compressor package within a space-constrained situation.

6. Results and discussion

6.1. Results

Five *GA* control parameters, including *pp*, *bit*, *pc*, *pm*, and $iter_{max}$, are used in the optimization process, where *pp* is the population number, *bit* is the chromosome length, *pc* is the crossover rate, *pm* is the mutation rate, and $iter_{max}$ is the extreme iteration. Two kinds of optimization, one for a pure tone noise used for validating the GA's reliability and the other for broadband noise elimination used in air compressor's venting noise, are described below.

Table 1. Ranges of design parameters for silencer A ~ silencer C.

Silencer Type	Range of design parameters
Silencer A	L_o = 0.35 (m); a = 0.0615 (m) KT_1:[0.005, 0.01]; KT_2:[0.005, 0.01]; KT_3:[0.0151, 0.0449]; KT_4:[0.0151, 0.0449]; KT_5:[0.1, 0.35]; KT_6:[1.5708, 3.1416]
Silencer B	L_o = 0.35 (m); a = 0.0615 (m) KT_1*:[0.1, 0.9]; KT_2*:[0.1, 0.9]; KT_3*:[0.0151, 0.0449]; KT_4*:[0.0151, 0.0449]; KT_5*:[0.5, 0.9]; KT_6*: [1.5708, 3.1416]; KT_7*:[0.005, 0.01]; KT_8*:[0.005, 0.01]
Silencer C	L_o = 0.35 (m); a = 0.0615 (m) KT_1**:[0.1, 0.9]; KT_2**:[0.1, 0.9]; KT_3**:[0.0151, 0.0449]; KT_4**:[0.0151, 0.0449]; KT_5**:[0.5, 0.9]; KT_6**: [1.5708, 3.1416]; KT_7**:[0.005, 0.01]; KT_8**:[0.005, 0.01]; RT_9**:[0.3, 0.7]

6.1.1. TL maximization at a targeted tone

The TL of silencer A is maximized at the target tone (300 Hz). By using Eqs. (13) and (18a) and applying the *GA* control parameters, silencer A is optimized for design data. As shown in Table 2, three *GA* parameters *pc*, *pm*, and $iter_{max}$ are gradually adjusted to achieve better optimization [21]. Table 2 illustrates that a better *GA* ensemble is obtained in the 13th, where *pp*, *bit*, *pm*, *pc*, and $iter_{max}$ are 120, 15, 0.05, 0.8, and 10,000, respectively. In Figs. 11−13, the better design data is substituted into the theoretical formula, and the obtained TL curve is related to many *GA* control parameters (*pm*, *pc*, and $iter_{max}$). As shown in Table 2 and Fig. 13, TL reaches maximum at the specified pitch at 300 Hz when using the best *GA* set (*pp* = 120, *bit* = 15, *pm* = 0.05, *pc* = 0.8, and $iter_{max}$ = 10,000). By using equations (14), (15), (18b), (18c) and applying the same set of *GA* control parameters, the optimal TL for silencer B and C at the selected 300 Hz tone are evaluated and presented in Table 3. By substituting the optimal design data into the theoretical formula, the optimal TL curves for silencers A-C are plotted in Fig. 14.

6.1.2. Minimization of broadband noise

The TL effect of silencers minimizes the broadband (0−3000 Hz) noise through them. The optimal design data for silencer A is performed using Eqs. (13) and (17a) during optimization with the same *GA* parameters (*pp* = 120, *bit* = 15 *pm* = 0.05, *pc* = 0.8, $iter_{max}$ = 10,000). Similarly, the optimized design data for silencer B and C are evaluated using Eqs. (14) & (17b) and Eqs. (15) & (17c), respectively, during the GA optimization process. The optimal design data of silencers A~C are shown in Table 4. By substituting the optimal design data into the

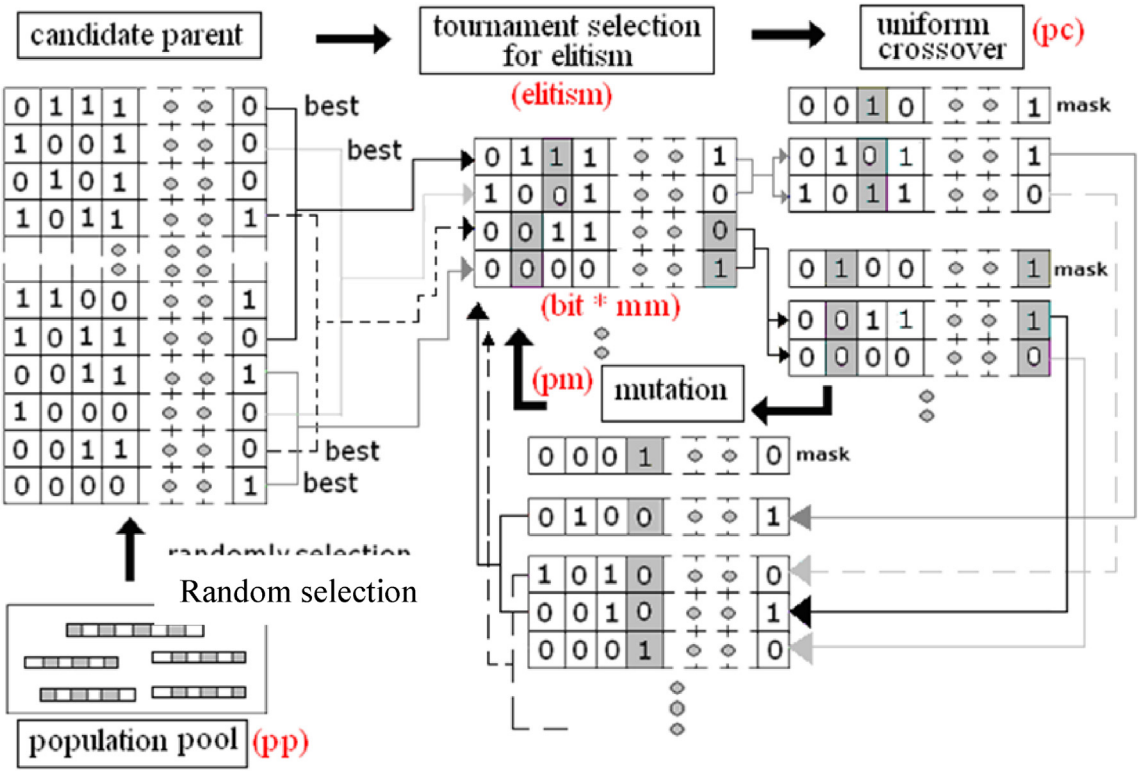

Fig. 9. Operations of the GA method.

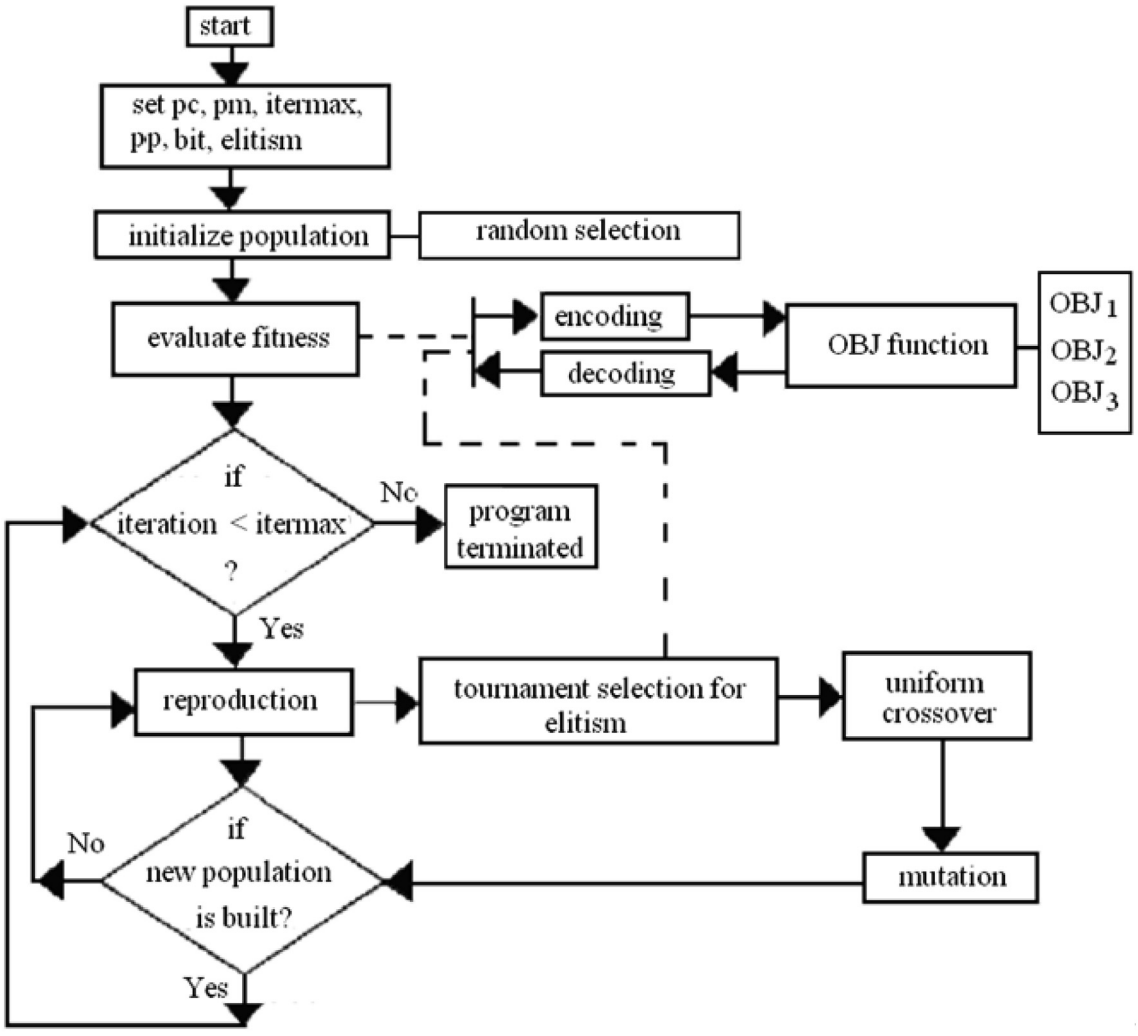

Fig. 10. Flowchart of the GA method.

theoretical formula, the optimal TL curves of silencers A~C are shown in Fig. 15.

6.2. Discussion

The TL maximization of the silencers A-C at the specified tone (300 Hz) is evaluated in section 6.1.1 to verify the reliability of the *GA*. The final design data and TL curves of silencers A-C are shown in Table 3 and Fig. 14. Figure 14 shows that the TL of the silencers is fully maximized at the desired tone (300 Hz) during *GA* optimization. Therefore, the genetic algorithm optimizer with silencer shape optimization is trustworthy. Furthermore, as shown in Table 3, the TLs of silencers A to C at the target tone (300 Hz) are 105.0 dB, 135.0 dB, and 135.0 dB, respectively. Silencer B and Silencer C are much better than Silencer A. Additionally, the TL curves of silencers B and C at the target tone are wider than that of silencer A, as shown in Fig. 14.

Optimization of silencers A-C is performed in section 6.1.2 to handle broadband discharge from space-constrained air compressors. The simulation results are provided in Table 4 and Fig. 15. Table 4 shows that the average deviations (between raw SWL and TL) for silencers A to C are 39.4 dB, 42.6 dB, and 49.9 dB, respectively. Silencer C is equipped with four straight cavities and one reverse cavity, which is superior to the others. In the study, silencer A with a reverse chamber has the worst sound attenuation. Also, as shown in Fig. 15, the TL curve of silencer C has the widest frequency band. However, it is worth noting that silencer A has a lower and narrower TL curve than the others.

To evaluate the acoustical influence from the geometric factors, a search of the TL regarding four dimensionless geometric factors (a_1/a, e_1/a, L_2/L_o, andθ/π) of silencer A is assessed and plotted in Fig. 16. To facilitate the parameter analysis, the

Table 2. Optimal design data for silencer A (silencer A: a circular silencer with one reverse chamber; pp = 120; bit = 15; targeted tone at 300 Hz).

Item	*GA* parameters			Results						OBJ
1	*pm*	*pc*	$iter_{max}$	KT_1	KT_2	KT_3	KT_4	KT_5	KT_6	*TL*(dB)
	0.01	0.2	100	0.005782	0.005782	0.01976	0.01976	0.1391	1.816	26.5
2	*pm*	*pc*	$iter_{max}$	KT_1	KT_2	KT_3	KT_4	KT_5	KT_6	*TL*(dB)
	0.01	0.4	100	0.00.7256	0.007256	0.02854	0.02854	0.2128	2.279	38.0
3	*pm*	*pc*	$iter_{max}$	KT_1	KT_2	KT_3	KT_4	KT_5	KT_6	*TL*(dB)
	0.01	0.6	100	0.009379	0.009379	0.04120	0.04120	0.3190	2.947	45.8
4	*pm*	*pc*	$iter_{max}$	KT_1	KT_2	KT_3	KT_4	KT_5	KT_6	*TL*(dB)
	0.01	0.8	100	0.009170	0.009170	0.03995	0.03995	0.3085	2.881	56.6
5	*pm*	*pc*	$iter_{max}$	KT_1	KT_2	KT_3	KT_4	KT_5	KT_6	*TL*(dB)
	0.01	0.9	100	0.009307	0.009307	0.04077	0.04077	0.3153	2.924	48.7
6	*pm*	*pc*	$iter_{max}$	KT_1	KT_2	KT_3	KT_4	KT_5	KT_6	*TL*(dB)
	0.03	0.8	100	0.008978	0.008978	0.03881	0.03881	0.2989	2.820	61.0
7	*pm*	*pc*	$iter_{max}$	KT_1	KT_2	KT_3	KT_4	KT_5	KT_6	*TL*(dB)
	0.05	0.8	100	0.009033	0.009033	0.03914	0.03914	0.3017	2.838	76.1
8	*pm*	*pc*	$iter_{max}$	KT_1	KT_2	KT_3	KT_4	KT_5	KT_6	*TL*(dB)
	0.07	0.8	100	0.009104	0.009104	0.03956	0.03956	0.3052	2.860	62.7
9	*pm*	*pc*	$iter_{max}$	KT_1	KT_2	KT_3	KT_4	KT_5	KT_6	*TL*(dB)
	0.09	0.8	100	0.008996	0.008996	0.03892	0.03892	0.2998	2.826	63.2
10	*pm*	*pc*	$iter_{max}$	KT_1	KT_2	KT_3	KT_4	KT_5	KT_6	*TL*(dB)
	0.05	0.8	200	0.009002	0.009002	0.03895	0.03895	0.3001	2.828	89.9
11	*pm*	*pc*	$iter_{max}$	KT_1	KT_2	KT_3	KT_4	KT_5	KT_6	*TL*(dB)
	0.05	0.8	1000	0.009049	0.009049	0.03923	0.03923	0.3024	2.843	91.7
12	*pm*	*pc*	$iter_{max}$	KT_1	KT_2	KT_3	KT_4	KT_5	KT_6	*TL*(dB)
	0.05	0.8	5000	0.009047	0.009047	0.03922	0.03922	0.3023	2.842	95.2
13	*pm*	*pc*	$iter_{max}$	KT_1	KT_2	KT_3	KT_4	KT_5	KT_6	*TL*(dB)
	0.05	0.8	10,000	0.009067	0.009067	0.03934	0.03934	0.3034	2.849	105.0

Notes: $KT_1 = a_1$; $KT_2 = a_2$; $KT_3 = e_1$; $KT_4 = e_2$; $KT_5 = L_2$; $KT_6 = \theta$

analyzed TL is set at 300 Hz. As indicated in Fig. 16, the TL is inversely proportional to a_1/a, the ratio of the inlet radius to the expansion chamber's radius. For geometric parameter e_1/a, where e_1 is the distance between the inlet and the expansion chamber and a is the expansion chamber's radius, the best TL occurs when e_1/a is 0.15. Also, the best TL occurs when the angle ratio of $\theta/\pi$is 0.15, where θ

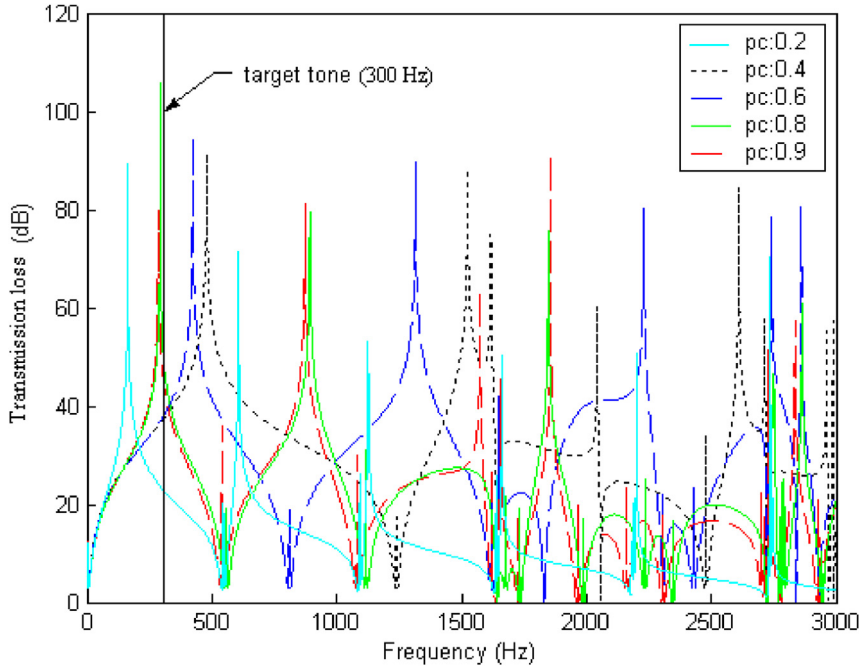

Fig. 11. Optimal TL with respect to the frequencies for a silencer with a one-chamber plug-inlet at various pc [pop = 120; bit = 15; pm = 0.01; $iter_{max}$ = 100; targeted frequency: 300 Hz].

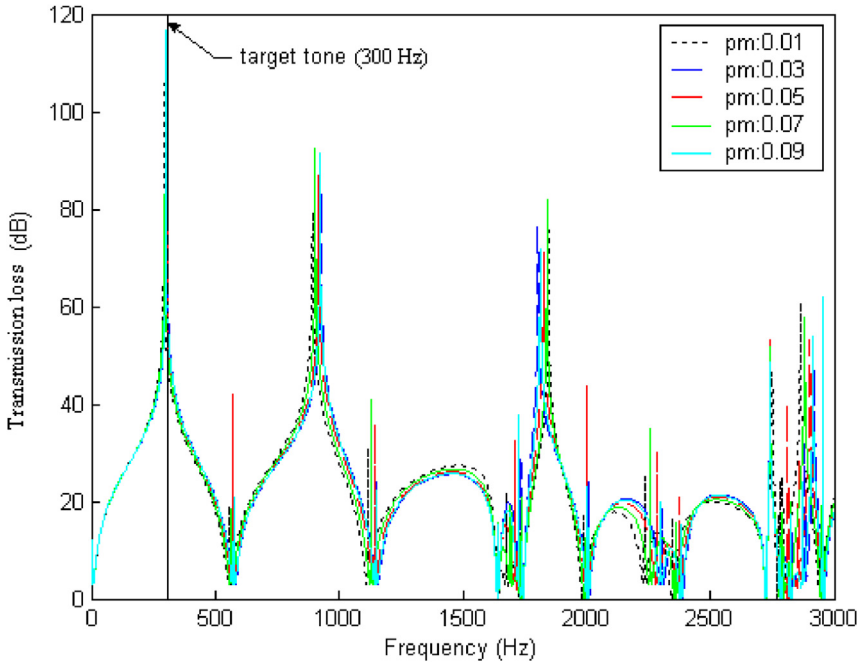

Fig. 12. Optimal TL with respect to the frequencies for a silencer with a one-chamber plug-inlet at various pm [pop = 120; bit = 15; pc = 0.8; $iter_{max}$ = 100; targeted frequency: 300 Hz].

is the angle between inlet and outlet and π is the angle of half-circle. Additionally, the best TL occurs when L_2/L_o is 0.83, where L_2 is the length of the chamber and L_o is a space-constrained length in the horizontal direction.

Subsequently, an examination of the TL about eight dimensionless geometric factors (aa_1/a, aaa_1/a, a_1/aa_1, a_2/aaa_1, e_1/a, L_1/L_o, L_2/L_o, and θ/π) of silencer B is conducted and presented in Fig. 17. As shown in Fig. 17, the TL is optimized when aa_1/a, the ratio of a

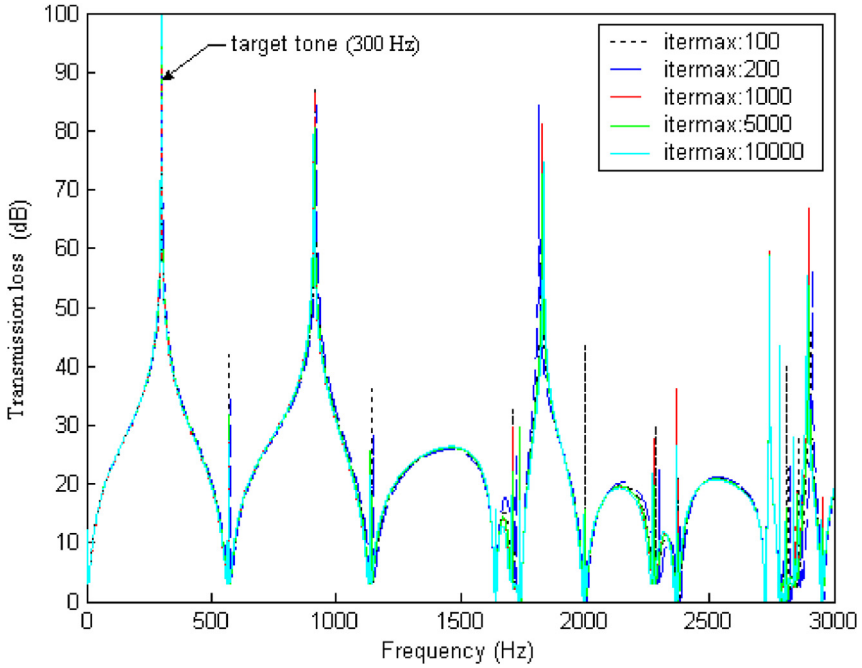

Fig. 13. Optimal TL with respect to the frequencies for a silencer with a one-chamber plug-inlet at various $iter_{max}$ [pop = 120; bit = 15; pc = 0.8; pm = 0.05; targeted frequency: 300 Hz].

Table 3. Optimal design data for three kinds of silencers (silencer A ~ silencer C) at target tone of 300 Hz (pp = 120; bit = 15; pm = 0.05; pc = 0.8; $iter_{max}$ = 15,000).

Silencer type	Design Parameters									*OBJ* -*STL*(dB)
Silencer A	KT_1 0.009067	KT_2 0.009067	KT_3 0.03934	KT_4 0.03934	KT_5 0.3034	KT_6 2.849				105.0
Silencer B	KT_1* 0.8068	KT_2* 0.8068	KT_3* 0.04143	KT_4* 0.04143	KT_5* 0.8534	KT_6* 2.959	KT_7* 0.009418	KT_8* 0.009418		135.1
Silencer C	KT_1** 0.8068	KT_2** 0.8068	KT_3** 0.04143	KT_4** 0.04143	KT_5** 0.8534	KT_6** 2.959	KT_7** 0.009418	RT_8** 0.009418	KT_9** 0.6534	135.0

Notes: $KT_1 = a_1$; $KT_2 = a_2$; $KT_3 = e_1$; $KT_4 = e_2$; $KT_5 = L_2$; $KT_6 = \theta$
$KT_1* = a_1/aa_1$; $KT_2* = a_2/aaa_1$; $KT_3* = e_1$; $KT_4* = e_2$; $KT_5* = L_2/Lo$; $KT_6* = \theta$;$KT_7* = aa_1$; $KT_8* = aaa_1$.
$KT_1** = a_1/aa_1$; $KT_2** = a_2/aaa_1$; $KT_3** = e_1$; $KT_4** = e_2$; $KT_5** = L_2/Lo$;$KT_6** = \theta$;$KT_7** = aa_1$; $KT_8** = aaa_1$; $KT_9** = L_1/(Lo- L_2)$.

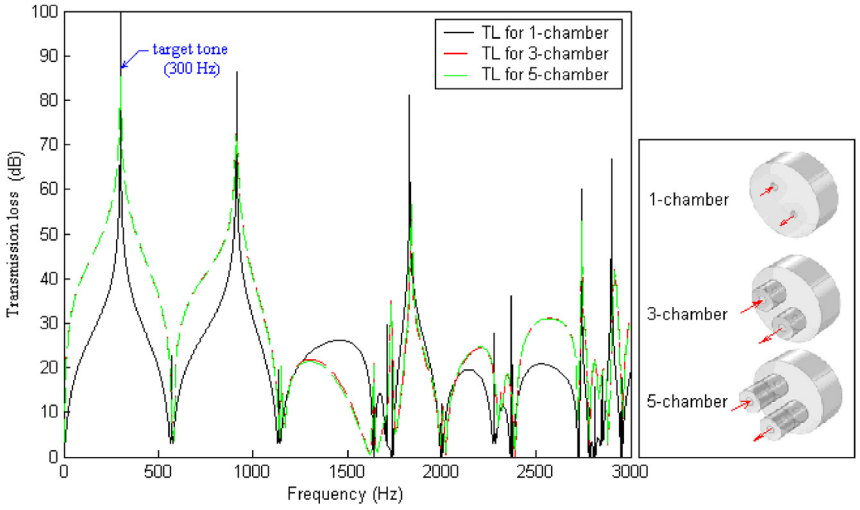

Fig. 14. Comparison of the TL with respect to various silencers at the targeted frequency of 300 Hz (pop = 120; bit = 15; pm = 0.05; pc = 0.8; $iter_{max}$ = 15,000).

Table 4. Optimal design data for three kinds of silencers (silencer A ~ silencer C) for broadband noise (pp = 120; bit = 15; pm = 0.05; pc = 0.8; $iter_{max}$ = 15,000).

Silencer type	Design Parameters									*OBJ*
Silencer A	KT_1 0.006694	KT_2 0.006694	KT_3 0.02519	KT_4 0.02519	KT_5 0.1847	KT_6 2.103				87.7
Silencer B	KT_1* 0.1008	KT_2* 0.1008	KT_3* 0.01513	KT_4* 0.01513	KT_5* 0.5004	KT_6* 1.572	KT_7* 0.005005	KT_8* 0.005005		84.5
Silencer C	KT_1** 0.1008	KT_2** 0.1008	KT_3** 0.01513	KT_4** 0.01513	KT_5** 0.5004	KT_6** 1.572	RT_7** 0.005005	KT_8** 0.005005	KT_9** 0.3004	77.2

Notes: $KT_1 = Lz/Lo$; $KT_2 = Lz1/Lz$; $KT_3 = D_1/Do$; $KT_4 = D_2/Do$; $KT_5 = Lc_1/Lz1$; $KT_6 = \eta_1$; $KT_7 = dh_1$.

reverse chamber's inlet radius relative to the expansion chamber's radius, or e_1/a is 0.15; or when $\theta/\pi = 0.2$ or a_1/aa_1, the ratio of expansion chamber's inlet radius relative to the reverse chamber's inlet radius, = 0.22 or $L_2/L_o = 0.65$, where L_2 is the length of the reverse chamber and L_o is a space-constrained length in the horizontal direction; or when L_1/L_o is 0.49, where L_1 is the length of the straight chamber and L_o is a space-constrained length in the horizontal direction. In addition, the TL reaches the minimum when aaa_1/a, the ratio of reverse chamber's outlet radius relative to the expansion chamber's radius, is 0.4. Furthermore, the TL slowly decreases as a_2/aaa_1, the ratio of the expansion chamber's outlet radius relative to the reverse chamber's outlet radius, increases.

Similarly, the effect of the TL relating to eight dimensionless geometric parameters (aa_1/a, aaa_1/a, a_1/aa_1, a_2/aaa_1, e_1/a, L_1/L_3, L_2/L_o, and θ/π) of silencer C is explored and shown in Fig. 18. As shown in Fig. 18, the TL is the maximum when aa_1/a is 0.15 or e_1/a is 0.15 or θ/π is 0.2 or a_1/aa_1 is 0.23 or L_2/L_o is 0.63.

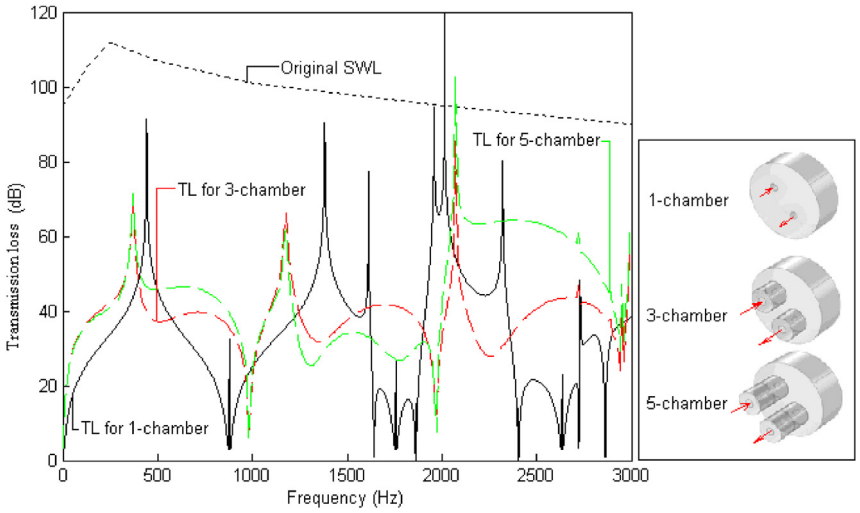

Fig. 15. Comparison of the TL with respect to various silencers [broadband noise].

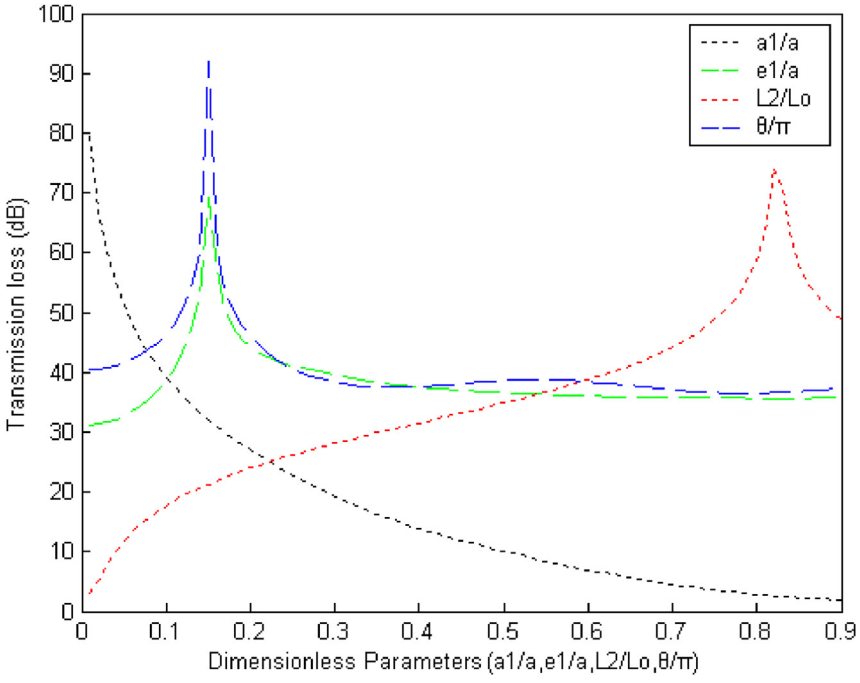

Fig. 16. Sensitivity analysis of dimensionless shape parameters for silencer A [at a specified frequency: 300 Hz].

The TL slowly increases as L_1/L_3, where L_1 is the inlet straight chamber's length and L_3 is the outlet straight chamber's length) increases. Consequently, the TL slowly decreases as a_2/aaa_1 increases.

7. Conclusion

An eigen function based on 3-D wave propagation and shown in Eqs. (1) and (2) is adopted and used in the derivation of a four-pole transfer matrix in Eq. (5). The system matrix is formed using the matrix multiplication of a reverse silencer hybridized with multiple straight chambers. The dependability of the *GA* optimizer is validated by using a single tone optimization before broadband noise optimization is implemented. To design an appropriate silencer that can efficiently reduce the broadband spectrum of the air compressor's SWL, a silenced overall sound power level (SWLT) is obtained by summing up individual silenced sound power levels (i.e., SWLOi-TLi for the ith octave band frequency) shown in Eq. (17) a, b, and c. The study result reveals that considering a limited space in the real world, the overall acoustical

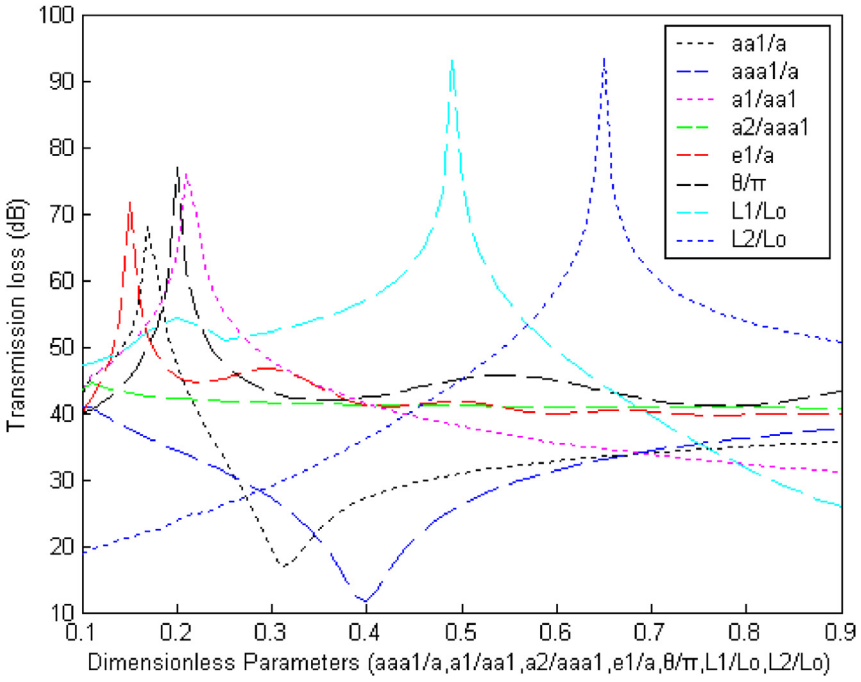

Fig. 17. Sensitivity analysis of dimensionless shape parameters for silencer B [at a specified frequency: 300 Hz].

efficiency increases as more straight chambers are mounted at both inlet and outlet of the reverse silencer. Also, the TL's profile widens as the number of straight chambers increases. A dimensionless geometric parameter analysis of silencers A-C is performed to appreciate the influence of the geometric parameters on the silencer's TL, as illustrated in Figs. 16−18. Resonant effects are observed for the circular multi-chamber reverse silencers. Consequently, considering a limited space in the real world, the shape optimization on circular silencers is internally installed with multiple reverse chambers using the objective function in conjunction with an optimization scheme.

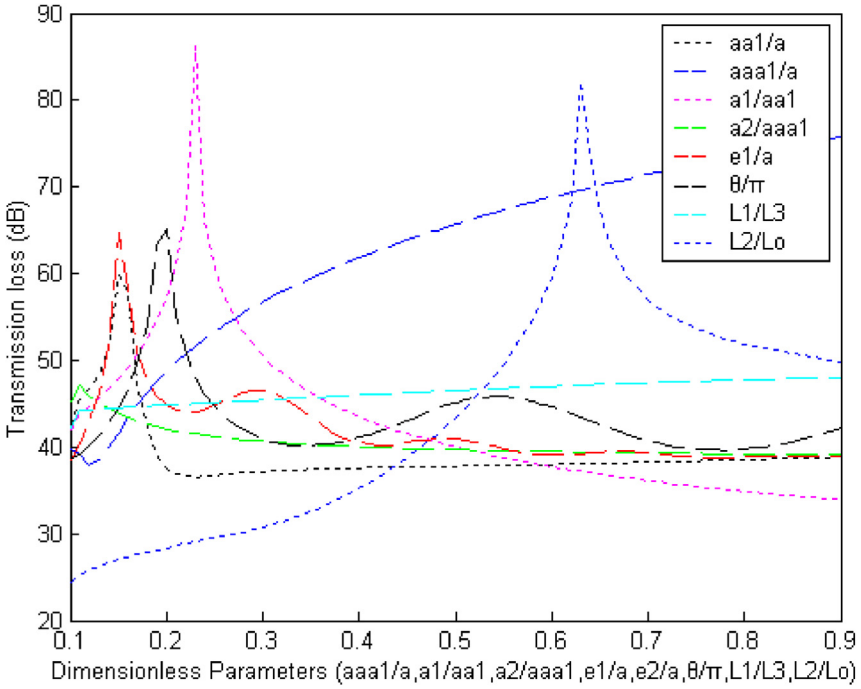

Fig. 18. Sensitivity analysis of dimensionless shape parameters for silencer C [at a specified frequency: 300 Hz].

Acknowledgements

The authors acknowledge the financial support of Ministry of Science and Technology (MOST (TW) 104-2221-E-036-027, ROC). We have no conflict of interest.

References

[1] Munjal ML. Velocity ratio-cum-transfer matrix method for the evaluation of a muffler with mean flow. J Acoust Soc Am 1957;39:105−19.
[2] Sullivan JW, Crocker MJ. Analysis of concentric-tube resonators having unpartitioned of cavities. J Acoust Soc Am 1978;64(1):207−15.
[3] Sullivan JW. A method for modeling perforated tube muffler components. I: theory. J Acoust Soc Am 1979;66(3):772−8.
[4] Ih JG, Lee BH. Analysis of higher-order mode effects in the circular expansion chamber with mean flow. J Acoust Soc Am 1985;77:1377−88.
[5] Yi SI, Lee BH. Three-dimensional acoustic analysis of a circular expansion chamber with side inlet and side outlet. J Acoust Soc Am 1986;79(5):1299−306.
[6] Yi SI, Lee BH. Three-dimensional acoustic analysis of a circular expansion chamber with side inlet and end outlet. J Acoust Soc Am 1987;81(5):1279−87.
[7] Ih JG, Lee BH. Theoretical prediction of the transmission loss of circular reversing chamber mufflers. J Sound Vib 1987;112: 261−72.
[8] Munjal ML. A simple numerical method for three-dimensional analysis of simple expansion chamber silencers of rectangular as well as circular cross-section with a stationary medium. J Sound Vib 1987;116:71−88.
[9] Selamet A, Ji ZL. Acoustic attenuation performance of circular flow-reversing chambers. J Acoust Soc Am 1998;104:2867−77.
[10] Mimani A, Munjal ML. Transverse plane-wave analysis of short elliptical end-chamber and expansion-chamber mufflers. Int J Acoust Vib 2010;15(1):24−38.
[11] Ranjbar M, Hardtke HJ, Fritze D, Marburg St. Finding the best design within limited time: a comparative case study on methods for optimization in structural acoustics. J Comput Acoust 2010;18(2):149−64.
[12] Siano D, Bozza F, Auriemma F. Acoustic and fluid-dynamic optimization of an automotive muffler. Proc Inst Mech Eng - Part D J Automob Eng 2012.
[13] Mimani A, Munjal ML. Acoustic end-correction in a flow-reversal end-chamber muffler: a semianalytical approach. J Comput Acoust 2016;24(1650004):1−44.
[14] Arslan H, Ranjbar M, Dalkõlõç B, Çalõk E, Arslan C. On muffler design for transmitted noise reduction. Journal of New Results in Science 2018;7(2):13−21.
[15] Mohamad B, Karoly J, Zelentsov A, Amroune S. A hybrid method technique for design and optimization of formula race car exhaust muffler. International Review of Applied Sciences and Engineering 2020;11(2):174−80.
[16] Arslan H, Ranjbar M, Secgin E, Celik V. Theoretical and experimental investigation of acoustic performance of multi-chamber reactive silencers. Appl Acoust 2020;157:106987.
[17] Arslan H, Ranjbar M, Mutlum Z. Maximum sound transmission loss in multi-chamber reactive silencers: are two chambers enough? ENG Transactions 2021;2:1−15.
[18] Mohamad B, Karoly J, Zelentsov A, Amroune S. Investigation of perforated tube configuration effect on the performance of exhaust mufflers with mean flow based on three-dimensional analysis. Arch Acoust Q 2021;46(3):561−6.
[19] Chiu MC. Optimal design of multi-chamber mufflers hybridized with perforated intruding inlets and resonated tube using simulated annealing. ASME J. of Vibration and Acoustics 2010;132:1−10.
[20] Chiu MC. Numerical assessment of reverse-flow mufflers using a simulated annealing method. The Canadian Society for Mechanical Engineering (CSME) Transactions 2010;34(1): 17−35.
[21] Chiu MC. Shape optimization of multi-chamber mufflers with plug-inlet tube on a venting process by genetic algorithms. Appl Acoust 2010;71:495−505.
[22] Chiu MC. Genetic algorithm optimization on a venting system with three-chamber hybrid mufflers within a constrained back pressure and space. ASME J. of Vibration and Acoustics 2012;134:1−11.
[23] Chiu MC. Numerical assessment of hybrid mufflers on a venting system within a limited back pressure and space using simulated annealing. J Low Freq Noise Vib Act Control 2011;30(4):247−75.
[24] Chiu MC. Numerical assessment for a broadband and tuned noise using hybrid mufflers and a simulated annealing method. J Sound Vib 2013;332:2923−40.
[25] Ranjbar M, Kemani M. A comparative study on design optimization of mufflers by genetic algorithm and random search method. Journal of Robotic and Mechatronic Systems 2016;1(2):7−12.
[26] Mohamad B, Karoly J, Zelentsov A, Amroune S. A comparison between hybrid method technique and transfer matrix method for design optimization of vehicle muffler. FME Transactions 2021;49(2):494−500.
[27] Siano D, Auriemma F, Bozza F. A correlation study of computational techniques of a three-pass perforated tube muffler including BEM and 1D methods. SEEP; 2009.
[28] Jones PW, Kessissoglou NJ. A numerical and experimental study of the transmission loss of mufflers used in respiratory medical devices. Acoust Aust 2010;38(1):13−9.
[29] Vasile O, Gillich N. Finite element analysis for reactive and dissipative rectangular muffler, Recent advances in signal processing," Computational Geometry and Systems Theory. 2011. p. 251−5.
[30] Vasile O, Gillich GR. Finite element analysis of acoustic pressure levels and transmission loss of a muffler," Advances in remote sensing, Finite Differences and Information Security. 2012. p. 43−8.
[31] Galphade A, Patil AV. Design and analysis of muffler for 800 cc car. International Journal of Advance Research in Engineering, Science & Technology 2015;2(7):72−6.
[32] Somashekar G, Prakasha AM, Ahamd N, Badrinarayan KS. Modal analysis of muffler of an automobile by experimental and numerical approach. International Journal of Recent Research in Civil and Mechanical Engineering 2015;2(1):309−14.
[33] Chiu MC, Chang YC. An assessment of high-order-mode analysis and shape optimization of expansion chamber mufflers. Arch Acoust Q 2014;39(4):1−11.
[34] Chiu MC, Chang YC. Shape optimization of multi-chamber side inlet/outlet mufflers hybridized with multiple perforated intruding tubes using genetic algorithm. J Mar Sci Technol 2013;21(3):238−49.
[35] Munjal ML. Acoustics of ducts and mufflers with application to exhaust and ventilation system design. New York: John Wiley & Sons; 1987.
[36] Holland J. Adaptation in natural and artificial system. Ann Arbor: University of Michigan Press; 1975.
[37] Jong D. An analysis of the behavior of a class of genetic adaptive systems, Doctoral thesis, Dept. Computer and Communication Sciences, Ann Arbor. University of Michigan; 1975.